Journal of the Optical Society of Korea, Vol. 5, No. 4, December 2001, pp. 140-145

Volumetric Interferometry Using Spherical Wave Interference for Three-Dimensional Coordinate Metrology

Hyug-Gyo Rhee, Ji-Young Chu, and Seung-Woo Kim*

Department of Mechanical Engineering, BUPE Creative Research Initiative Group, Korea Advanced Institute of Science and Technology, Daejeon 305-701, KOREA

(Received September 10, 2001)

We present a new method of volumetric interferometer, which is intended to measure the three-dimensional coordinates of a moving object in a simultaneous way with a single optical setup. The method is based on the principles of phase-measuring interferometry with phase shifting. Two diffraction point sources, which are made of the polished ends of single-mode optical fibers are embedded on the object. Two spherical wavefronts emanate from the diffraction point sources and interfere with each other within the measurement volume. One wavefront is phase-shifted by elongating the corresponding fiber using a PZT extender. A CCD array sensor fixed at the stationary measurement station detects the resulting interference field. The measured phases are then related to the three-dimensional location of the object with a set of non-linear equations of Euclidean distance, from which the complete set of three-dimensional spatial coordinates of the object is determined through rigorous numerical computation based upon the least square error minimization.

OCIS codes : 060.2380, 120.3180, 120.5050.

I. INTRODUCTION

Coordinate measuring machines (CMMs) for precision dimensional metrology have long been designed with three orthogonal measurement axes equipped with linear optical encoders or heterodyne laser interferometers. This Cartesian coordinate approach of the CMMs design suffers a significant loss of measurement accuracy because of the so-called parallax errors that are caused by large Abbe offsets between the measurement axes and the probe [1]. The Abbe offsets vary with the position of the probe within the measurement volume and the angular motion errors of slide ways change with the fluctuation in environmental temperature. Due to these reasons, it is not easy to completely eliminate the parallax errors by adopting metrology frames and/or software compensation technique that is based upon deterministic error models. Furthermore, the recently established self-calibration technique of using periodic grid artifacts has limited effectiveness because it is at present feasible only for the two-dimensional calibration of planar motion. Consequently, the volumetric uncertainty of the orthogonal type CMMs is ultimately limited by the geometrical imperfection of slide ways, of which current level is in the range of a few micrometers at best in a working volume of about half a cubic meter.

One attempt being made in recent years is the so-called multi-lateration, which aims to reduce the parallax errors by taking non-orthogonal parallel-mechanism structures wherein measurement axes are directly connected to the probe to minimize Abbe offsets. This multi-lateration determines the three-dimensional coordinates of the probe by solving inverse kinematics of the measured diagonal distances of the probe from several fixed points. However, there are many difficult practica problems that are encountered in fabricating CMMs of this sort, because small geometrical defects existing in the sphere joints of measurement axes usually surpass all the advantages small Abbe offsets provided by adopting non-orthogonal structural designs. Another approach of multi-lateration for CMM applications is to measure the diagonal distances of the probe by using tracking laser interferometers along with retro-reflectors. Avoiding troublesome rotating joint mechanisms requires wide view-angle retro-reflectors to send the measuring laser beam exactly back to the incoming direction regardless of the orientation of the reflector. In this case, the measuring uncertainty of CMMs is determined solely by the stability of the laser interfer-

ometer system and machine structure, provided that the geometrical errors of retro-reflectors may be neglected [2], [3], [4].

Here in this paper, we present a new scheme of multi-lateration using a volumetric interferometer system that relies upon the principles of phase-shifting phase-measuring interferometry in contrast with other multi-lateration techniques that use multiple tracking laser interferometers. The probe holds two diffraction point sources, which are made of the polished ends of single-mode optical fibers. Two spherical wavefronts emanate from the diffraction point sources and they interfere with each other within the working volume, while one wavefront is phase-shifted by elongating the corresponding fiber using a PZT extender. The resulting interference field is detected by a two-dimensional CCD array of photo-detectors that are fixed at the stationary measurement station. The phase information captured by the photo-detectors is related to the three-dimensional coordinates of the probe with a set of non-linear equations of Euclidean distances, from which the spatial coordinates of the probe are determined by rigorous numerical computation of least square error minimization. A prototype measurement system is designed and tested to find out the level of measurement precision within a working volume of side 100 mm.

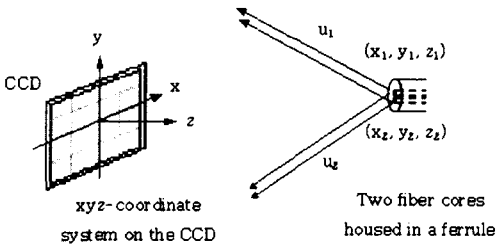

(a) Basic geometry for volumetric interferometer.

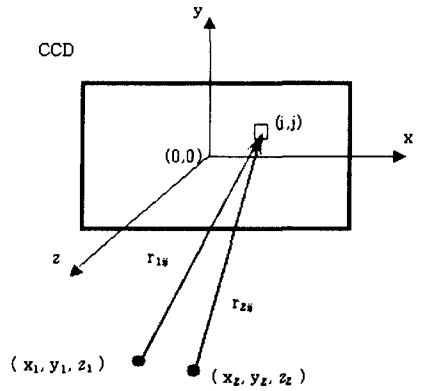

(b) xyz-coordinates for pixels on the CCD array.

FIG. 1. Basic configuration for the volumetric interferometer.

II. PRINCIPLES OF VOLUMETRIC INTERFEROMETRY

When an optical fiber of single mode propagation emits light into free space, it acts like a pinhole that brings forth a spherical wavefront with its origin located right at the core center of the fiber exit. The effective core diameter of the single mode fiber is in the range of 2 to 3 μm, which is much smaller than the size of conventional pinholes that are typically on the order of 10 μm, being limited by fabrication difficulties. In addition, the phase distribution across the cross section of the fiber end is intrinsically uniform and the intensity distribution maintains the Gaussian HE11 mode [5]. These superior characteristics of the single mode fiber as a pinhole offer an almost perfect spherical wavefront without the use of additional optics such as condensing and collimating lenses [6].

Fig. 1 illustrates the basic geometric configuration of the volumetric interferometer proposed in this investigation. It comprises two optical fibers of single mode and a CCD sensor of two-dimensional photodetector array. The two fibers are aligned with their ends side by side with an inter-axis distance of 125 mm and fixed on the object whose spatial position is to be measured. The CCD sensor is secured stationary on the machine frame. The xyz-measurement coordinate system is set on the plane of the CCD sensor, and the origins of the two spherical waves are expressed with six unknown coordinates such as (x_1,y_1,z_1) and (x_2,y_2,z_2), respectively. The two spherical wavefronts from the fibers interfere with each other and generate a time-invariant intensity field across the measurement volume. The primary task of the volumetric interferometer is to identify the six unknown coordinates by detecting the intensity information of the interference fringes formed on multiple discrete pixel points of the CCD sensor. Once this is successfully done, the identified six coordinates lead to the complete determination of the spatial position of the object holding the fibers in six degrees of freedom, i.e., three translational plus three rotational motions.

The electric amplitudes of the wavefronts that reach the CCD pixels from the two optical fibers, designated fiber 1 and fiber 2 for distinction, are expressed as

$$u_{1ij} = \frac{A_{1ij}}{r_{1ij}} e^{-j(kr_{1ij}+\phi_1)},$$

where

$$r_{1ij} = \sqrt{(x_1 - i * F_1)^2 + (y_1 - j * F_2)^2 + z_1^2} \quad (1)$$

and

$$u_{2ij} = \frac{A_{2ij}}{r_{2ij}} e^{-j(kr_{2ij}+\phi_2)},$$

where

$$r_{2ij} = \sqrt{(x_2 - i * F_1)^2 + (y_2 - j * F_2)^2 + z_2^2}. \quad (2)$$

The subscripts i and j index the individual locations of the CCD pixels, and F_1 and F_2 are the spacing distances between the two adjacent pixels in the x and in the y directions, respectively. In addition, r_{1ij} and r_{2ij} are the Euclidean radial distances from the fibers to the CCD pixels, k is the wave number, and ϕ_1 and ϕ_2 are the initial phases measured right at the origins of the two wavefronts. The intensity distribution of the interference of the above two spherical wavefronts on the CCD pixels is then worked out as

$$I_{ij} = |u_{1ij} + u_{2il}|^2 = \Pi_{ij} + \Gamma_{ij} cos[\Phi_{ij}], \quad (3)$$

where

$\Pi_{ij} = \frac{A_{1ij}^2}{r_{1ij}^2} + \frac{A_{2ij}^2}{r_{2ij}^2}, \Gamma_{ij} = 2\frac{A_{1ij}A_{2ij}}{r_{1ij}r_{2ij}}, \Phi_{ij} = k(r_{1ij} - r_{2ij}) + \delta\phi, \delta\phi = \phi_1 - \phi_2$.

The phase Φ_{ij} of the interference intensity I_{ij} depends on the distance difference between r_{1ij} and r_{2ij} and also on the initial phase difference between ϕ_1 and ϕ_2. The value of Φ_{ij} is measured by using the phase-shifting method, which is implemented by elongating one of the optical fibers using a tube type PZT extender. In computing Φ_{ij}, we use the A-bucket algorithm that is capable of compensating for the phase shift errors that are inevitably encountered due to the imprecision of fiber elongation [7].

The initial phase difference $\delta\phi$ that is contained Φ_{ij} is unknown, but it remains constant for all the pixels. So, $\delta\phi$ is removed along with the wave number k by defining the new variable Λ_{ij} such as

$$\Lambda_{ij} = \frac{\Phi_{ij} - \Phi_{00}}{k} = (r_{1ij} - r_{2ij}) - (r_{100} - r_{200}). \quad (4)$$

Λ_{ij} represents the difference of the distances from the pixel (i,j) to the origins of the optical fibers, where the pixel (0,0) located at the center of the CCD array is taken as the reference. Then the six unknowns of (x_1, y_1, z_1) and (x_2, y_2, z_2) are determined so as to best fit the model of Eq.(3) to the measured data of Λ_{ij}. For this, the cost function to be minimized is defined as.

$$E = \Sigma_{ij}(\Lambda_{ij} - \hat{\Lambda}_{ij})^2. \quad (5)$$

where $\hat{\Lambda}_{ij}$ denotes the actual measured value of Λ_{ij}, and the summation of Σ_{ij} is performed over all the pixels. The cost function E turns out to be highly nonlinear in terms of the unknowns of (x_1, y_1, z_1) and (x_2, y_2, z_2). Thus the numerical technique is used to search for the global minimum of the cost function, from which the solutions of the unknowns are finally obtained. The numerical search for the global minimum requires two appropriate algorithms; one is for determining the search direction in the multi-dimensional space of the six unknowns and the other is for determining the step size of the search. The modified Newtons method based on the BFGS algorithm is elected for the search direction, which offers a relatively high computational speed when the number of unknowns is moderate [8], [9]. The step size is determined using the Amijo method [10] along with the 3rd-order polynomial fitting [11].

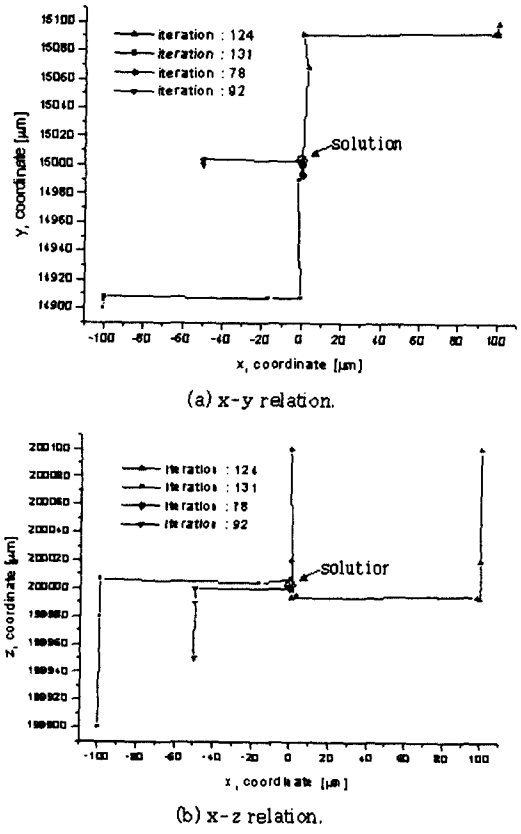

FIG. 2. Convergence of the numerical search for the global minimum.

Fig. 2 shows an exemplary result of the computer simulation that was performed to verify the suitability of the selected numerical search algorithms. For simulation, the unknowns (x_1, y_1, z_1) and (x_2, y_2, z_2) were assumed to be located exactly at (0, 15, 200) and (-0.125, 15, 200) with all the dimensions in millimeters, and the phase Φ_{ij} was computed using the interference intensity model of Eq.(3). Then, assuming the computed values of Φ_{ij} as the measured data, the true solutions of the unknowns were found out with the search algorithms. The initial guesses for the unknowns were varied with diverse offsets in the range of 100 μm from the true locations. As shown in the figure, regardless of the initial guesses, the global mi-

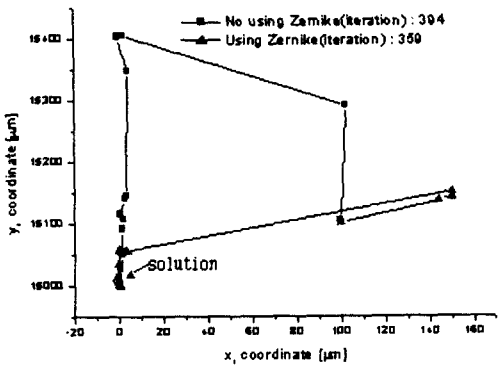

(a) x-y relation.

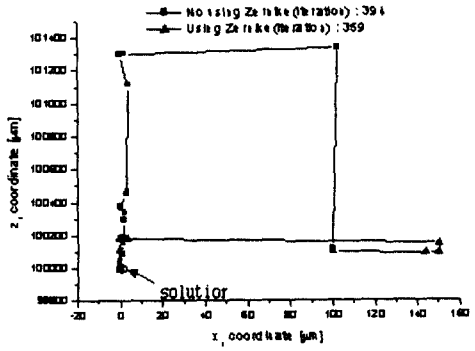

(b) x-z relation.

FIG. 3. Reduction of the total number of iterations.

nimum was always reached within about 130 iterations. This type of simulation was repeated for different true locations of the unknowns, which confirms the search algorithm yields a robust convergence. The computation time is greatly affected by the initial guesses of the unknowns, from which the numerical search starts. The computation time can be reduced by using the relationship between $(x_1,\ y_1,\ z_1)$ and $(x_2,\ y_2,\ z_2)$, because they are not independent of each other. Λ_{ij} of Eq.(4) may be expanded from the origin of the xyz-coordinates system such as

$$\Lambda_{ij} = \Lambda_{ij}|_{i=0,j=0} + \frac{\partial \Lambda_{ij}}{\partial i}|_{i=0,j=0} i + \frac{\partial \Lambda_{ij}}{\partial j}|_{i=0,j=0} j + \frac{\partial^2 \Lambda_{ij}}{\partial i \partial j}|_{i=0,j=0} ij + ... \quad (6)$$

$$= 0 + (\frac{x_2}{r_{200}} - \frac{x_1}{r_{100}})i + (\frac{y_2}{r_{200}} - \frac{y_1}{r_{100}})j + (\frac{x_2 y_2}{r_{200}^3} - \frac{x_1 y_1}{r_{100}^3})ij + ...$$

On the other hand, the measured $\hat{\Lambda}_{ij}$ may be fitted into the Zernike polynomials such as

$$\hat{\Lambda}_{ij} = \Sigma_n \alpha_n Z_n(i,j) = \alpha_0 + \alpha_1 i + \alpha_2 j + \alpha_3 ij + ... \quad (7)$$

Comparing Eq.(7) with Eq.(6) permits $(x_2,\ y_2,\ z_2)$ to be expressed in terms of $(x_1,\ y_1,\ z_1)$ such as

$$x_2 = r_{200}(\alpha_1 + \frac{x_1}{r_{100}}), y_2 = r_{200}(\alpha_2 + \frac{y_1}{r_{100}}),$$
$$z_2 = \sqrt{r_{200}^2 - x_2^2 - y_2^2}, \quad (8)$$

where
$r_{200} = \frac{(\alpha_1 + \frac{x_1}{r_{100}})(\alpha_2 + \frac{y_1}{r_{100}})}{2\alpha_3 + \frac{x_1 y_1}{r_{100}^3}}$.

Thus, the initial guesses for (x_2,y_2,z_2) are not made arbitrary, but they are estimated from the initial guesses of (x_1,y_1,z_1) along with the coefficients α_0, α_1, α_2, and α_3 of the Zernike polynomials fitted from the measured $\hat{\Lambda}_{ij}$ as in Eq.(7). Fig 3. shows that the total number of iterations in numerical search can be reduced by using the relations of Eq.(8).

III. VOLUMETRIC INTERFEROMETER CONSTRUCTION AND ERROR ANALYSIS

Figs. 4 and 5 show the overall hardware configuration of the volumetric interferometer proposed in this investigation. A beam frin a HeNe laser with

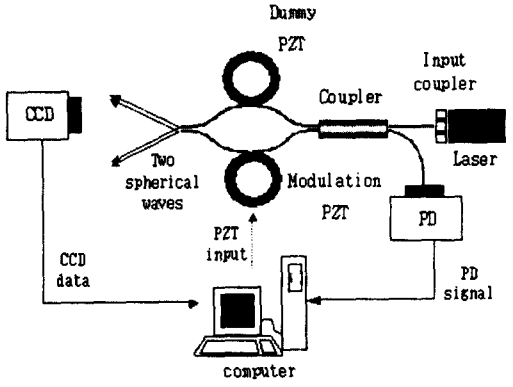

FIG. 4. Optical configuration of the volumetric interferometer.

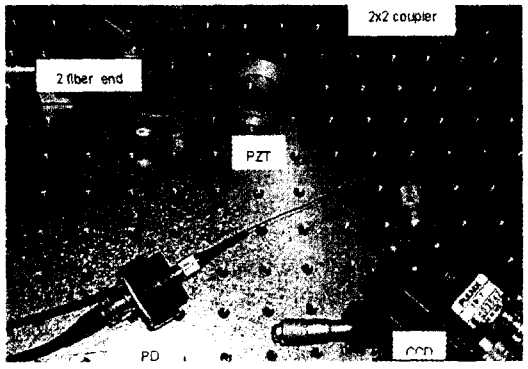

FIG. 5. Experimental setup.

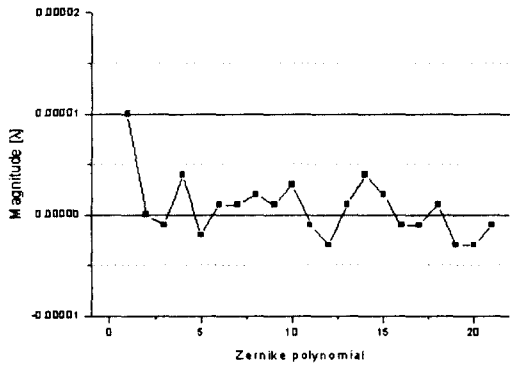

FIG. 6. Verification of sphericity.

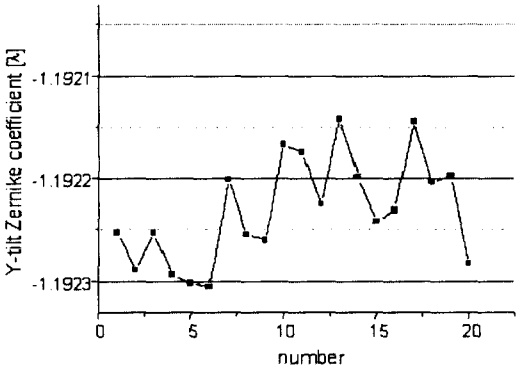

FIG. 7. Measurement repeatability of the volumetric interferometer.

632.8 nm wavelength is fed to a single mode fiber through an input coupler. Then the fiber is connected to a 2x2 coupler that divides the input beam by 50:50 into two branches. Each branch fiber is wound around a PZT extender that elongates the length of the fiber to induce phase shift. At the ends of the fibers, two spherical wavefronts are emitted to the CCD array. About 4 % of the total emitting light is reflected from the ends of the fibers, which is monitored by a photodetector attached to an input end of the 2x2 coupler. The reflected beams interfere with other, which provides the information on the difference of the initial phases of the emitting fibers. The CCD camera has a two-dimensional array of 640 x 480 photodetectors, which has a spacing of 8.44 μm in the x direction, while 9.78 μm in the y direction.

The pixels of the CCD array have a finite size of rectangular shape. Thus, the sampled intensity from a pixel is in fact an average, not the intensity value precisely measured at the center of the pixel as is assumed in the subsequent phase-measuring computation. However, thorough analysis reveals that the effect of the finite size of pixels on the measurement error is negligible. On the other hand, the actual sphericity of the interfering wavefronts significantly affects the measurement error. The sphericity can be verified as follows: Firstly, for a given relative geometry between the CCD array and the emitting fibers, the six coordinates of (x_1, y_1, z_1) and (x_2, y_2, z_2) are determined following the principles of volumetric interferometry described in the previous section. Secondly, using the determined six coordinates of the fibers, two ideal spherical wavefronts are virtually generated by simulation, from which the ideal phase values for all the CCD pixels are subsequently computed. Finally, the deviation between the actual measured phases and the ideal simulated phases is evaluated.

As an example, Fig. 6 shows an experimental result when six coordinates are determined as (14917.3, 5873.1, 210302.5) and (14793.1, 5872.4, 210304.9) in micrometers. The deviation over the entire set of CCD pixels is fitted to the Zernike polynomials, whose computed coefficients are evaluated to be less than 1.5 x $10^{-5}\lambda$. This result is equivalent to a sphericity error of 7.63 nm in peak to valley and 0.61 nm in root-mean-squares. This type of verification is repeated by varying the positions of the fibers within the measurable volume. In our investigation, the maximum sphericity error is found in the range of 10 nm in maximum. It should be noted that the maximum sphericity error has a contribution of the repeatability of the search algorithms of determining the six coordinates of the emitting fibers, so the actual maximum sphericity is estimated better than the measured value.

The measurement repeatability of the volumetric interferometer is evaluated through twenty consecutive measurements. The measured phases of all the CCD pixels are fitted to the Zernike polynomials, among which the y-tilt component is found to be the dominant contribution to the measurement repeatability. Fig. 7 shown a plot of the y-tilt, which fluctuates with a peak-to-valley value of 0.000163 λ. The repeatability measured in terms of the coordinates (x_1, y_1, z_1) is (4.88, 5.03, 17.09) μm in peak-to-valley.

IV. CONCLUSIONS

A new design concept of high precision CMM has been presented by introducing a volumetric interferometer system that is capable of measuring the complete spatial motion of the probe in six degrees of freedom with no influences from the Abbe offsets and angular motion errors of slide ways. The volumetric interferometer operates on the principles of phase-shifting phase-measuring interferometry, which comprises two optical fibers held on the probe emitting two identical monochromatic spherical wavefronts and a CCD photodetector array monitoring the interference intensity of the two spherical wavefronts. The

xyz-coordinates of each fiber end are then determined so as to minimize the least square errors of the actual phase values computed from the intensity distribution sampled by the photodetector array. The prototype measurement system built in this investigation demonstrates that the measurement repeatability is in the level of 30 nm and the one-dimensional uncertainty is about 0.2 μm in a working distance of 150 mm. This concept of new design allows the CMM measurement to be free from Abbe offsets and angular motion errors in machine axes.

V. ACKNOWLEDGMENTS

The work published here has been conducted as part of the national project of Billionth Uncertainty Precision Engineering sponsored by the Ministry of Science and Technology of Korea as part of the Creative Research Initiatives Program.

*Corresponding author : swk@kaist.ac.kr.

REFERENCES

[1] J. B. Bryan, Precision Eng. **1**, 129 (1979).
[2] O. Nakamura, M. Goto, K. Toyoda, Y. Tanimura, and T. Kurosawa, Ann. CIRP **40**, 523 (1991).
[3] O. Nakamura and M. Goto, Appl. Opt. **33**, 31 (1994).
[4] E. B. Hughes, A Wilson, and G. N. Peggs, Ann. CIRP **49**, 391 (2000).
[5] A. Ishimaru, *Electromagnetic wave propagation, radiation, and scattering* (Prentice-Hall, Inc., 1991), 156.
[6] S. Kimura and T. Wilson, Appl. Opt. **30**, 2143 (1991).
[7] I. B. Kong and S. W. Kim, Opt. Eng. **34**, 183 (1995).
[8] A. D. Belegundu and T. R. Chandrupatla, *Optimization concepts and applications in engineering* (Prentice-Hall, Inc., 1999),74.
[9] P. E. Gill and W. Murray, J. Inst. Maths. Applns. **9**, 91 (1972).
[10] J. E. Dennis and R. B. Schnabel, *Numerical methods for unconstrained optimization and nonlinear equations* (Prentice-Hall, Inc., 1983), 1163.
[11] T. R. Chandrupatla, Computer Methods in Applied Mechanics and Engineering **152**, 211 (1999).